Journal of Solid State Chemistry **146,** 202–210 (1999)
Article ID jssc.1999.8334, available online at http://www.idealibrary.com on IDEAL®

From $Nb_{12}O_{29}$ to $Nb_{22}O_{54}$ in a Controlled Environment High-Resolution Microscope

M. J. Sayagués and J. L. Hutchison[1]

Department of Materials, University of Oxford, Parks Road, Oxford, OX1-3PH, United Kingdom

Received September 15, 1997; in revised form March 19, 1999; accepted April 21, 1999

A nonstoichiometric $Nb_{12}O_{29}(NbO_{2.417})$ block structure oxide with monoclinic symmetry was slightly oxidized in a controlled environmental high-resolution electron microscope. This instrument is based on a JEOL 4000 EX electron microscope equipped with a unique gas reaction cell in which the oxide could be oxidized by introducing O_2 at pressures up to 30 mbar, while promoting local reaction by electron beam heating. The oxidation process was seen to start in the regions where some stacking faults perpendicular to the c axis appear (in which the structure has local orthorhombic symmetry). The initial movement of atoms, involving a formation of lamellar defects, could be traced with great certainty. Such defects provide empty rectangular tunnels, similar to those found in the $NaNb_{13}O_{33}$ structure, which is a (4 × 3) block structure with Na cations situated in the rectangular tunnels. This stage of the oxidation reaction implies a minimal rearrangement, usually involving a simple unit jump (the primitive diffusion step) by atoms in certain sites. Then, the cooperative unit jumps along rows of atoms propagate the transformation through the crystal. A further stage in the oxidation gives rise to the $Nb_{22}O_{54}(NbO_{2.455})$ structure in some areas of the crystal, which could be identified in the high-resolution transmission electron microscopy image as well as in the electron diffraction patterns.

INTRODUCTION

High-resolution transmission electron microscopy (HREM) has, since Wadsley and co-workers (1) first started to investigate niobium oxides, become increasingly significant for the determination of local atom arrangement in complex oxides (2, 3). Recent advances in instrumentation for HREM have resulted in direct observation of structural changes on the atomic scale. However, most studies of solid state reactions have been confined to investigations of crystals that have undergone reaction. Information about reaction mechanisms is thus obtained *a posteriori*, i.e., after the event.

A controlled environment high-resolution electron microscope (4) offers the exciting possibility of analyzing directly the structural changes occurring during a solid state reaction, at the unit cell level, while a reaction is being carried out in the microscope. We have recently developed such a system, in which a gas-reaction cell is incorporated inside the objective lens polepiece of a JEOL 4000EX high-resolution electron microscope, operating at 400 kV, with 0.25 nm resolution.

An idealized projection of the $Nb_{12}O_{29}$ block structure (monoclinic variant) is shown in Fig. 1. This structure was described in detail in a previous paper (5), where a reaction study was performed, with the conclusion that the oxidation process occurred in two steps. First, lamellar defects with rectangular tunnels appeared, and secondly, the formation of a new block structure, $Nb_{10}O_{25}$ (i.e., $NbO_{2.500}$) was noted. However, subsequent oxidation experiments on the same material have led to clearer results from which we can

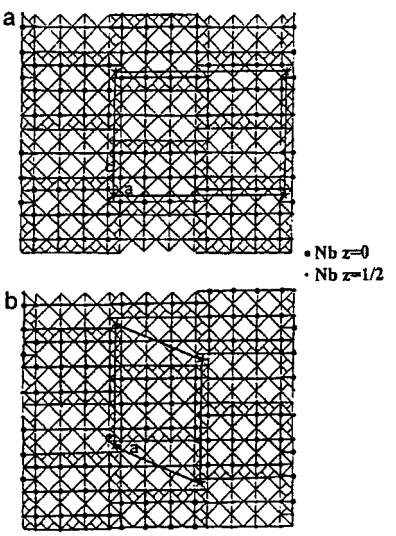

FIG. 1. Structure of (a) orthorhombic and (b) monoclinic $Nb_{12}O_{29}$, shown as linked blocks of corner-shared NbO_6 octahedra. Unit cells are outlined.

[1] To whom correspondence should be addressed.

0022-4596/99 $30.00

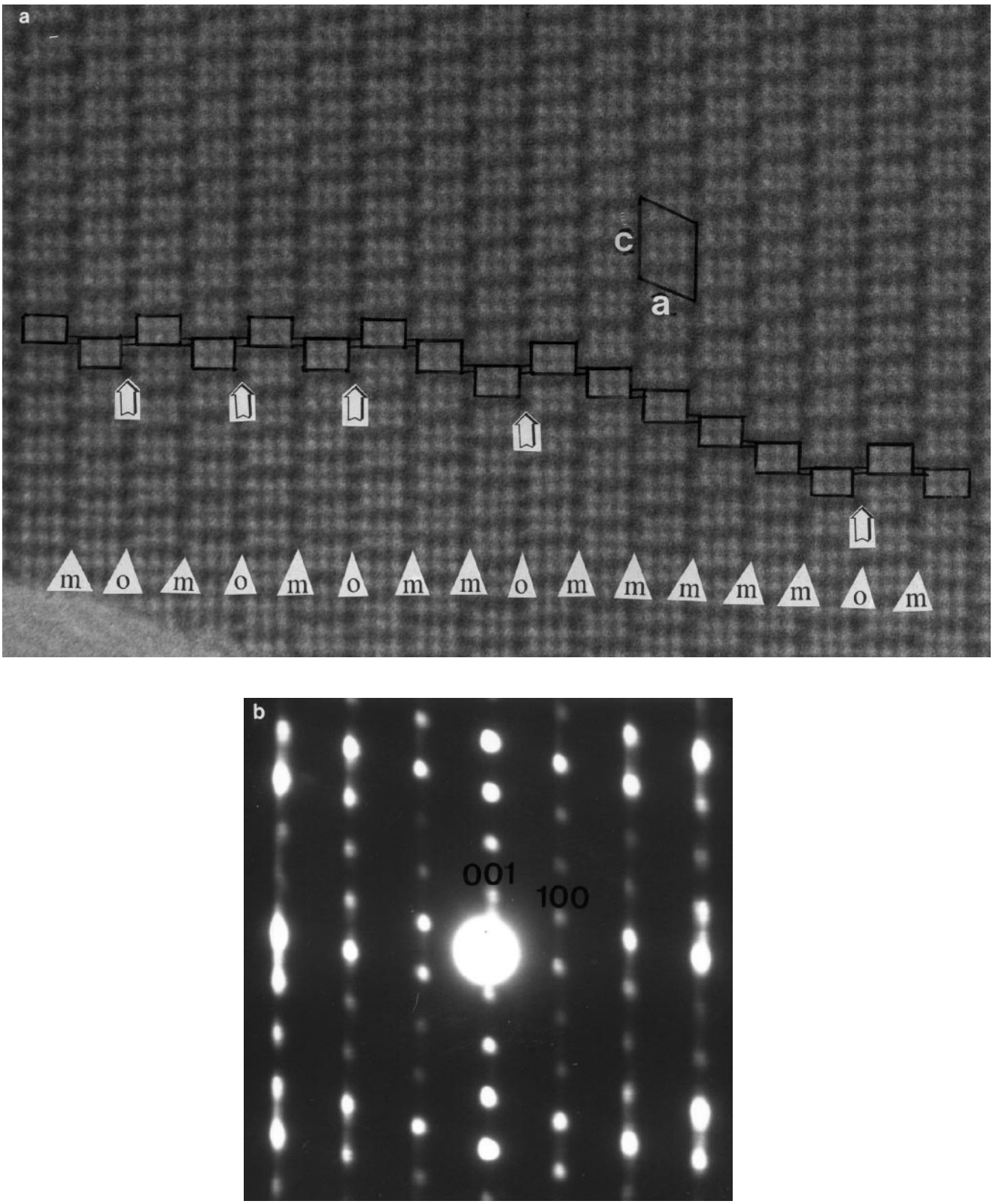

FIG. 2. (a) Micrograph of a $Nb_{12}O_{29}$ crystal under vacuum, viewed along [010]; (b) corresponding SAED pattern.

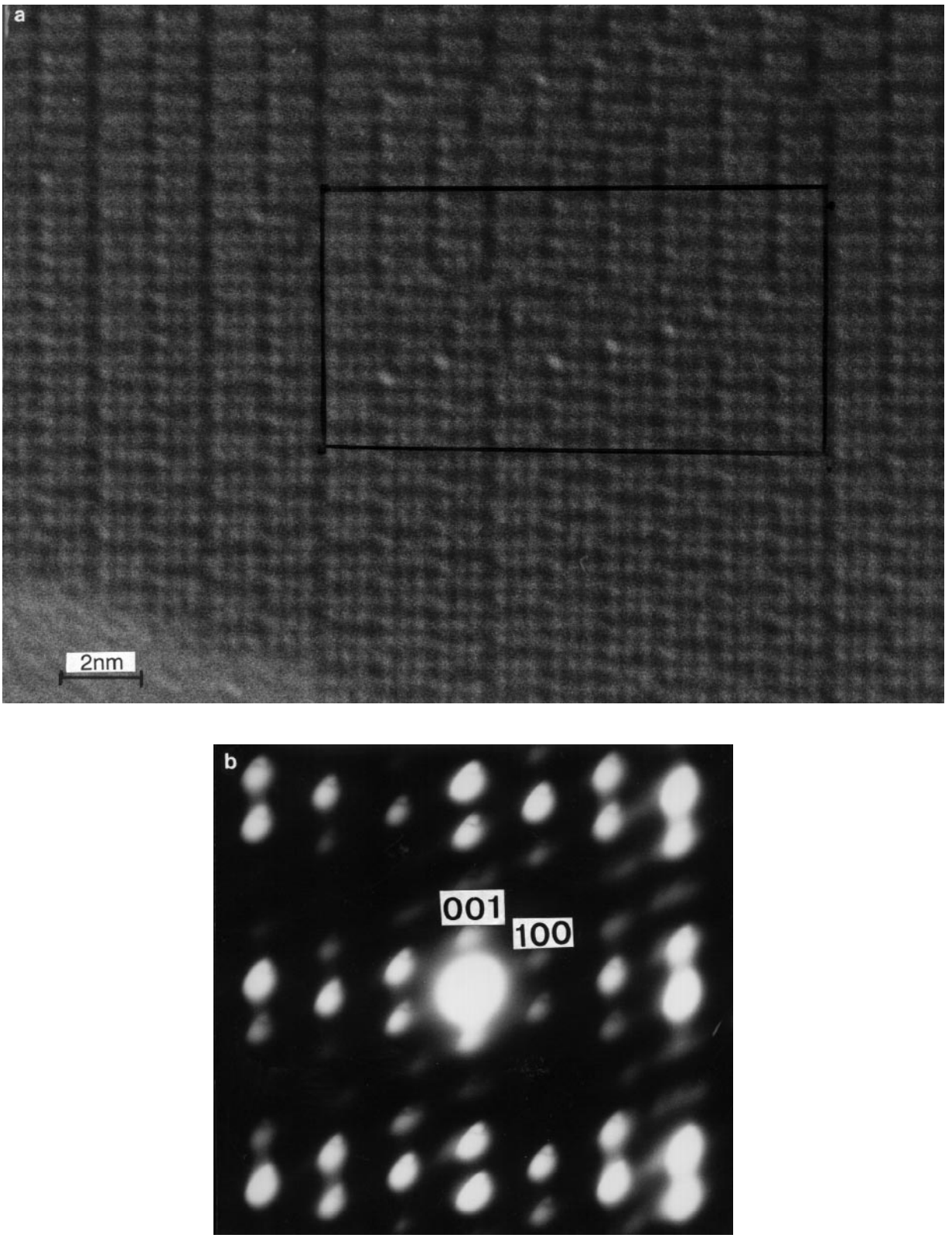

FIG. 3. (a) Micrograph from the above crystal (same area) after oxidation; (b) corresponding SAED. The marked area is mapped in Fig. 5.

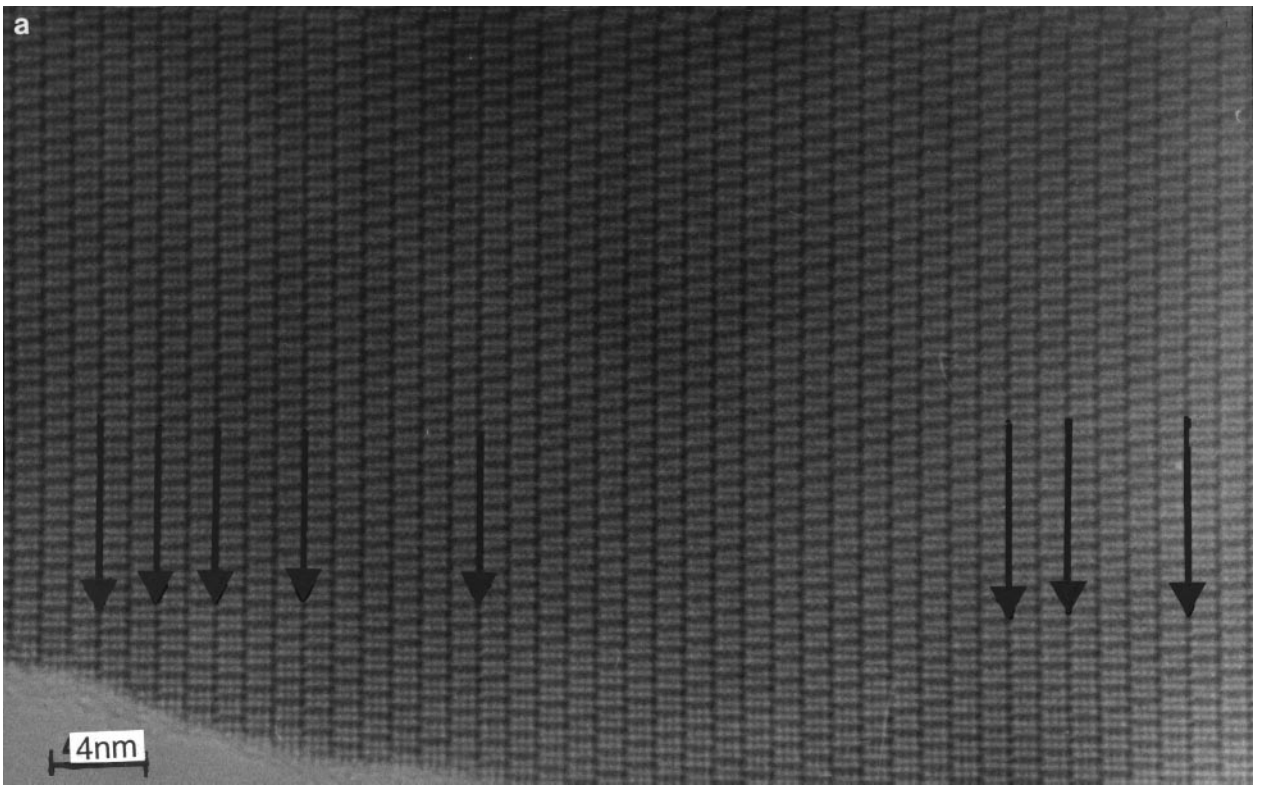

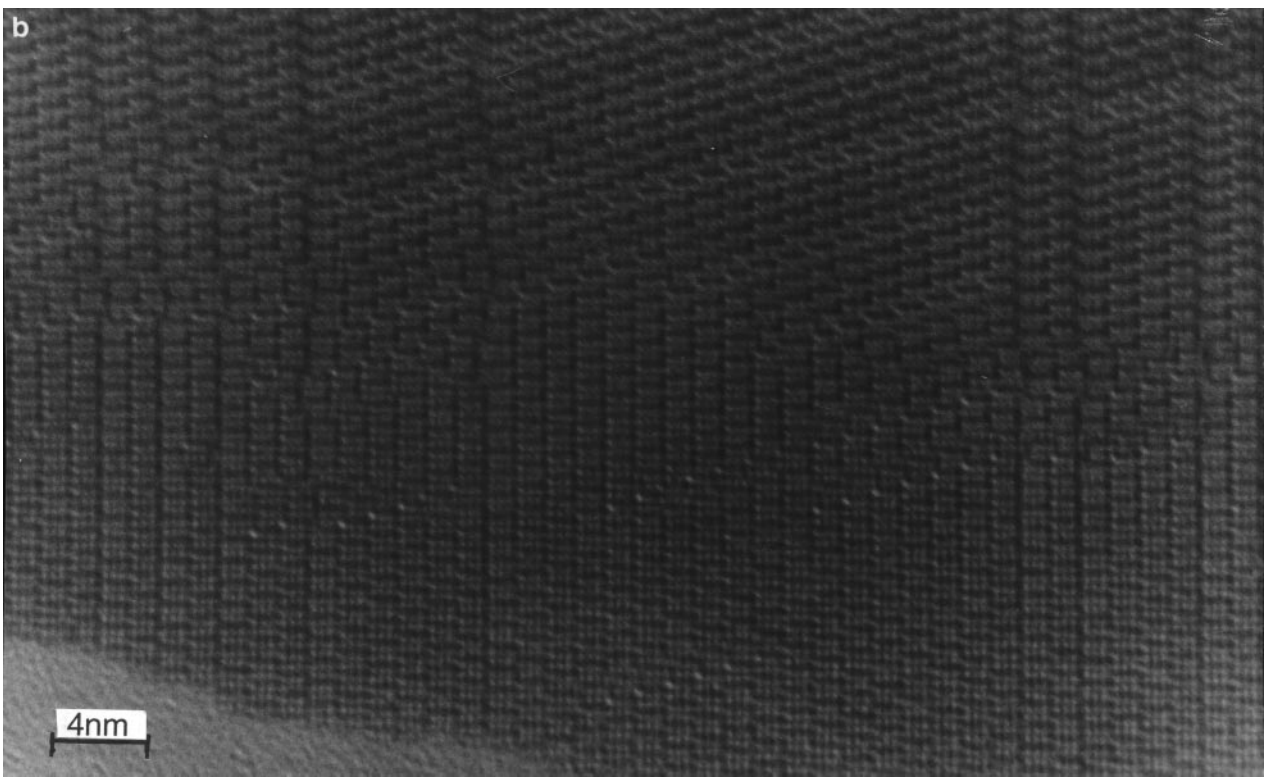

FIG. 4. Micrographs from the above crystal (a) under vacuum and (b) after oxidation. The coincident arrows show the stacking faults in the original structure and the ripple lines after oxidation.

now explain the mechanism involving single movements of atoms. In this paper, we will show the analysis of such results.

EXPERIMENTAL

Samples for HREM were prepared by dispersing a suspension of the $Nb_{12}O_{29}$ powder in acetone and evaporating a droplet onto a holey carbon film supported by a copper grid. Observations were made using the JEOL 4000 EX gas-reaction cell microscope (4) (side-entry configuration), the microscope being operated at 400 kV with a LaB_6 filament. A double-tilt specimen holder was used to orient thin crystallites with the **b** axis of the monoclinic cell parallel to the electron beam. Electron beam heating was used so that individual crystallites could be reacted in stages (rather than the whole specimen, which would be the case if a heating holder had been employed). Oxygen gas was admitted to the specimen area by means of a needle valve, at pressures up to 30 mbar.

Suitable crystals were located with the cell under vacuum and orientated in the [010] zone axis. Later, the oxygen gas was introduced into the specimen area and the electron beam was used (by changing the condenser aperture) to heat the crystal. The images were recorded at magnification 300,000× and 400,000× close to Scherzer defocus; at this defocus setting it is feasible to interpret HREM images of Nb oxide block structures intuitively, since these are well known to behave as phase objects, i.e., columns of cations along the **b** axis are imaged with dark contrast.

RESULTS AND DISCUSSION

The $Nb_{12}O_{29}$ monoclinic structure can be clearly visualized in the micrograph shown in Fig. 2a with the corresponding selected area electron diffraction (SAED) pattern in Fig. 2b. Observing carefully the white dot contrast in the micrograph (corresponding to the channels in the structure), it is possible to detect some stacking faults (marked with arrows). These can alternatively be described as monoclinic blocks joined to each other in an orthorhombic way in the direction perpendicular to the **c** axis. The sequence of stacking is depicted by letters "m" (monoclinic stacking) and "o" (orthorhombic stacking) along the bottom of the micrograph.

Oxygen (15 mbar) was introduced into the cell for 10 min and then the same area of the crystal was imaged. The micrograph and corresponding SAED pattern can be seen in Figs. 3a and 3b. Some structural changes are evident, which seem to start in lines parallel to the **c** axis (marked with arrows) exactly where the monoclinic blocks were joined in an orthorhombic manner, i.e., marked by arrows in Fig. 2. Figures 4a and 4b show a larger area of the crystal before and after oxidation, showing the coincidence between the ripples parallel to the **c** axis produced after oxidation and the stacking faults in the original structure. It seems to be that the oxidation starts to produce changes in the sites where the structure has some local defects (as, for instance, stacking faults).

The first movement of atoms gives place to lamellar defects $Nb_{11}O_{27}$ ($NbO_{2.450}$) in different areas, producing

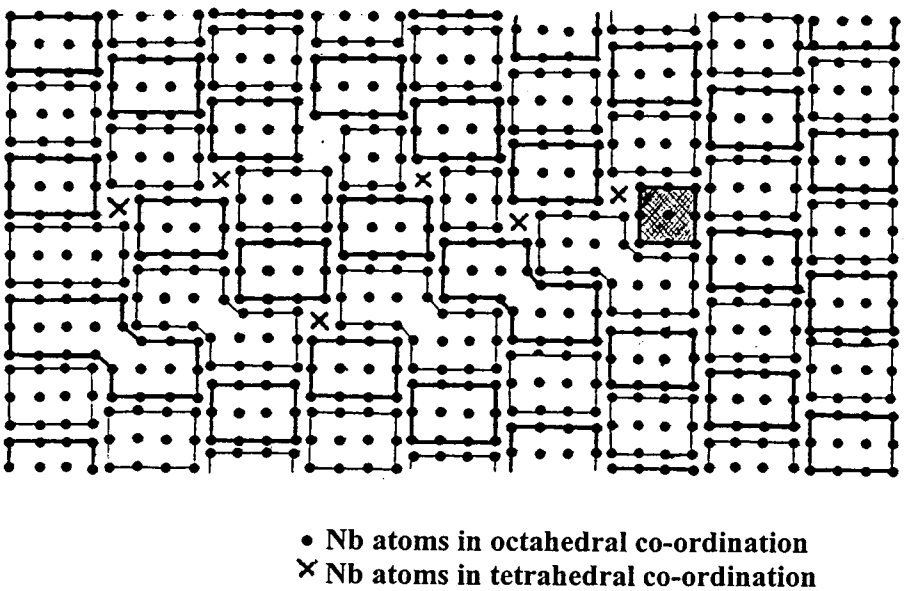

FIG. 5. Schematic representation of the block structure from the marked area in Fig. 2a. Cations only are shown. •, octahedral coordination, ×, tetrahedral coordination.

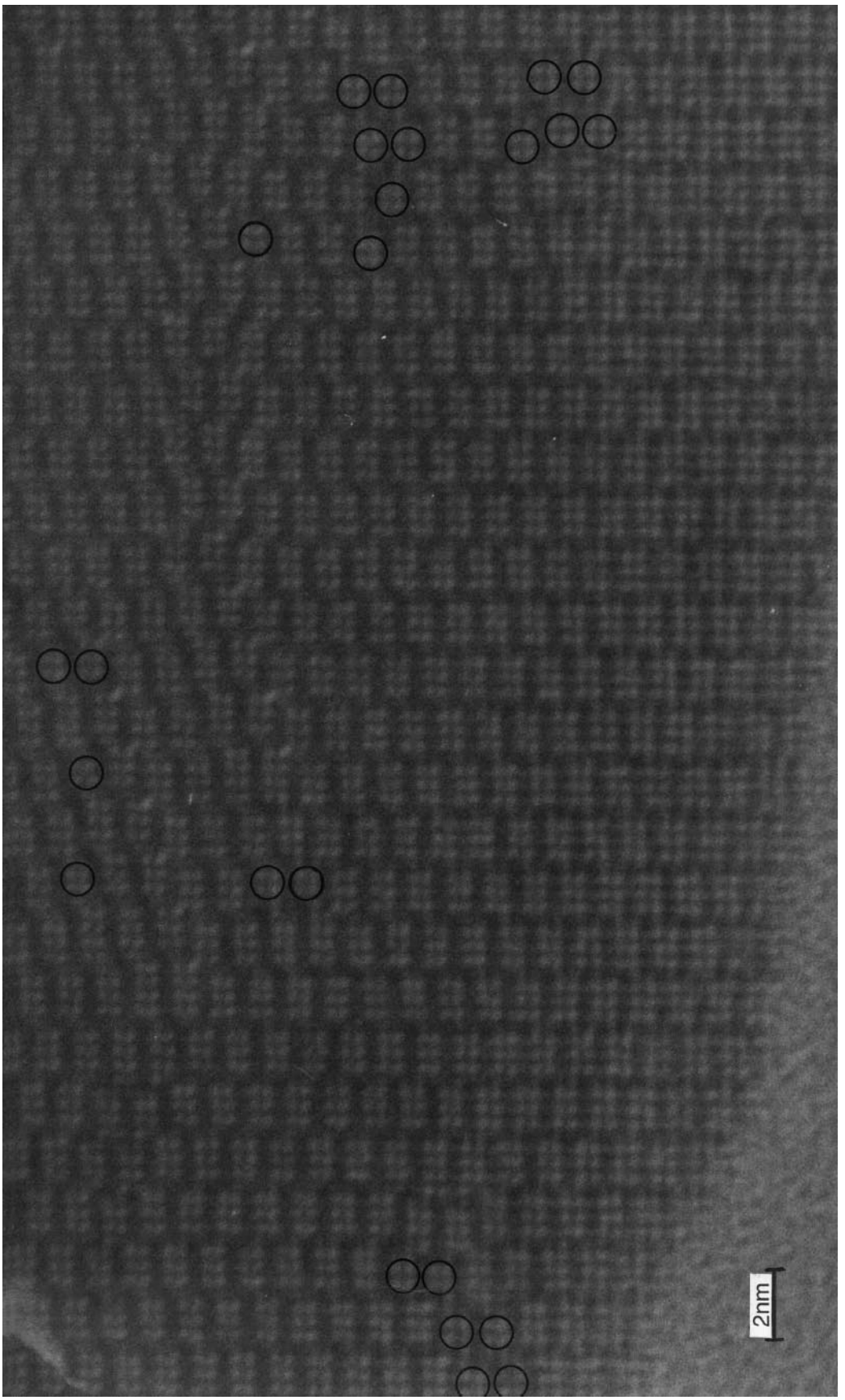

FIG. 6. Micrograph of the same crystal (same area) after further oxidation. (3×3) blocks are marked with open circles.

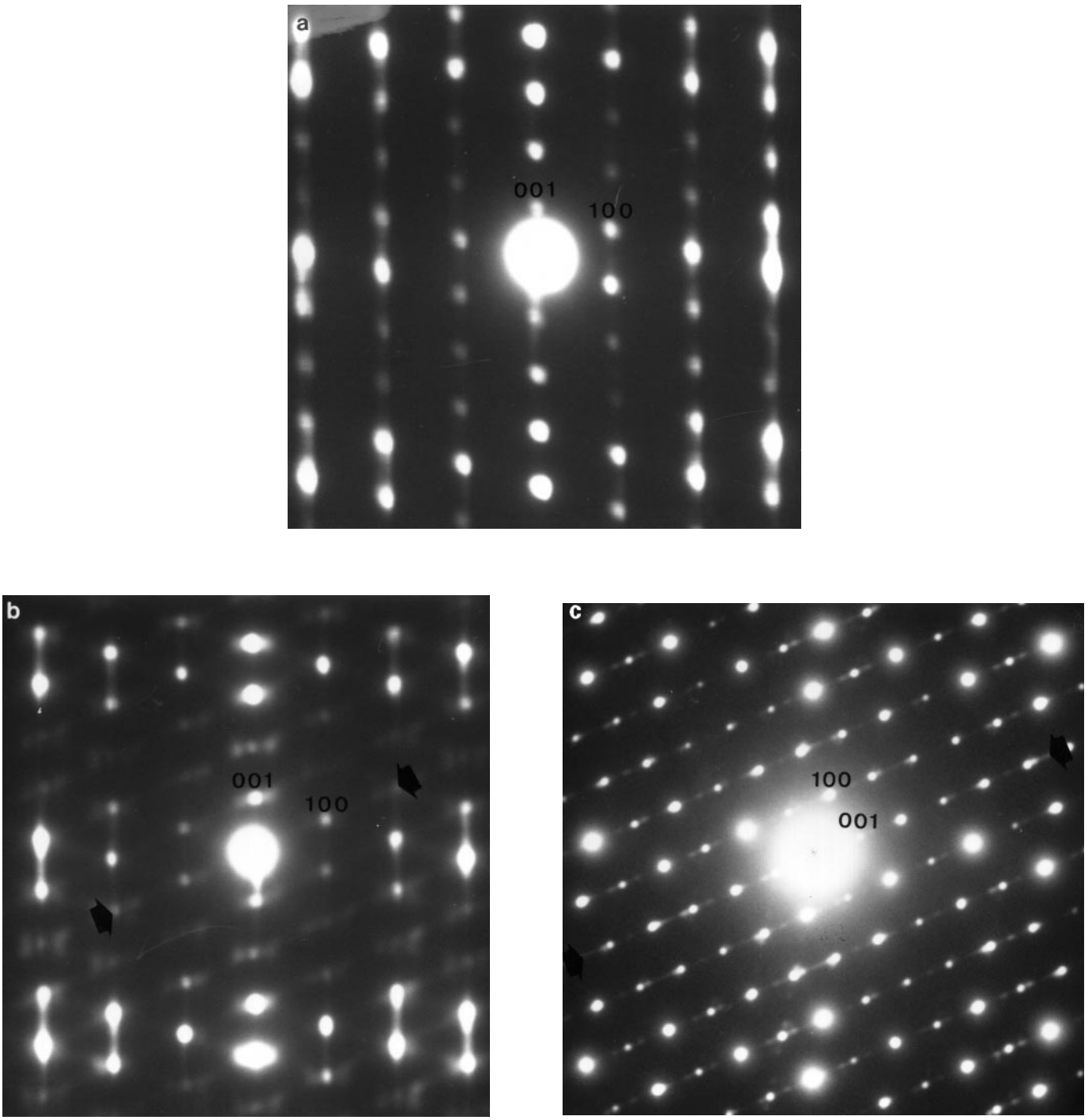

FIG. 7. SAED patterns of (a) the above crystal in vacuum, (b) the same crystal, same area after further oxidation, and (c) a $Nb_{22}O_{54}$ crystal in vacuum.

elongated white contrast in the micrograph due to the formation of rectangular tunnels produced when two blocks are linked in the [100] direction. This lamellar defect is very similar to that found in the $NaNb_{13}O_{33}$ [$(Na,Nb)O_{2.357}$] structure (6), although in that particular structure the rectangular tunnels are occupied by Na cations. The marked area in Fig. 3a is mapped in Fig. 5 where the cation movements can be seen clearly. Each line of the propagation of reaction appears to start with the formation of a (5×3) block. The displacement of the block interface can then be

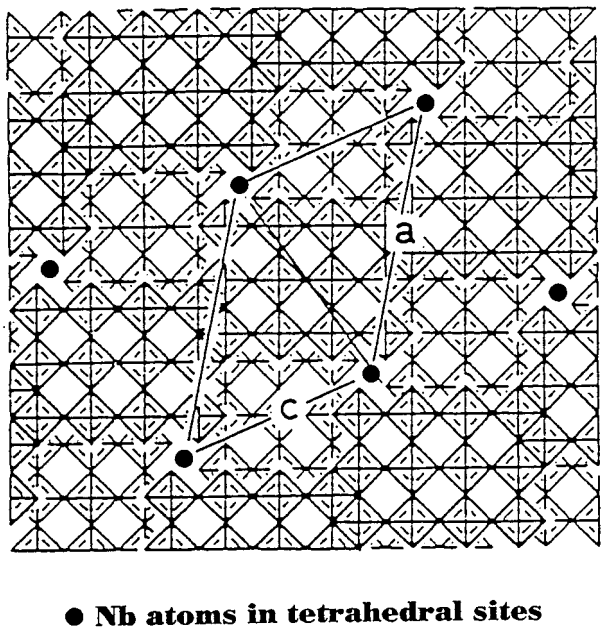

FIG. 8. Schematic representation of the $Nb_{22}O_{54}$ crystal structure (6) ($a = 2.12$ nm; $c = 1.06$ nm).

propagated in either direction from this, leading to ripples, which can be clearly seen in the micrograph. There must consequently be some other defect structure with (3×3) blocks at the end of the lamellar defect, which can also be observed in the micrograph. These are shaded in Fig. 5 and correspond to individual units of $Nb_{10}O_{25}$ (i.e., $NbO_{2.500}$) representing locally complete oxidation.

Further oxidation and heating were carried out on the same area, the resulting micrograph being shown in Fig. 6. The black contrast along the ripples (parallel to the **c** axis) has almost disappeared. However, different changes can be observed, which are marked with open circles. These small domains of (3×3) blocks interleaved with (4×3) blocks indicate that the formation of the $Nb_{22}O_{54}$ ($NbO_{2.454}$) structure has already begun. The black contrast corresponding to Nb^{5+} in tetrahedral sites can also be observed.

To confirm the formation of the $Nb_{22}O_{54}$ structure, the corresponding SAED pattern is shown in Fig. 6b, which is compared with the SAED patterns of the same $Nb_{12}O_{29}$ crystal in vacuum in the same area (Fig. 6a) and a $Nb_{22}O_{54}$ crystal in vacuum (Fig. 7c). The streaking evident in Fig. 6b

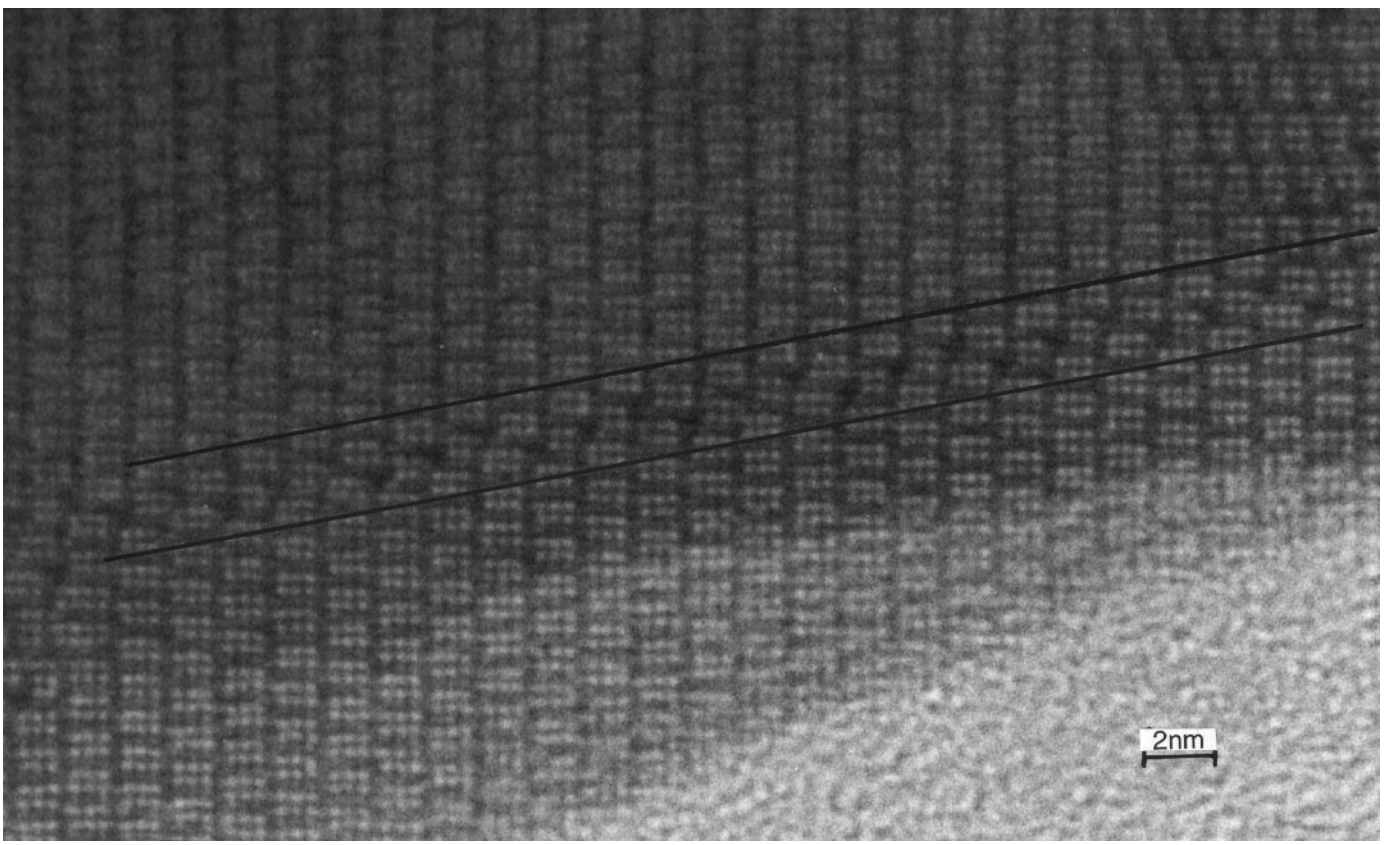

FIG. 9. Micrograph showing the same $Nb_{12}O_{29}$ crystal in another area after second oxidation. The $Nb_{22}O_{54}$ structure is marked between two lines; the black contrast corresponds to Nb^{5+} in tetrahedral sites.

seems to be in the same direction as that in the [001] $Nb_{22}O_{54}$ structure (Fig. 6c).[2]

The $Nb_{22}O_{54}$ structure (Fig. 8) can be considered as an intergrowth of $Nb_{12}O_{29}$ ($NbO_{2.417}$) and $Nb_{10}O_{25}$ ($NbO_{2.500}$). It is a block structure with tetrahedral sites occupied by Nb^{5+}. It can also be described as being formed by ribbons of linked (4×3) blocks alternating with rows of isolated (3×3) blocks.

Figure 9 shows a different area of the same crystal after the second oxidation. A row of (3×3) blocks and black contrast dots corresponding to the tetrahedral sites can be very clearly observed (marked between two lines). Therefore, these changes can be interpreted as an indication of local $Nb_{22}O_{54}$ structure formation in some areas of the crystal.

CONCLUSIONS

It is significant that the *in situ* oxidation process of $Nb_{12}O_{29}$ starts *away* from the edge of the crystal, taking place first in thicker regions. This suggests an easy diffusion of oxygen along the channels between octahedra into the middle. The initial creation of the lamellar defects—rectangular channels—would facilitate this diffusion. Also, from the fact that ordering appears to be preserved along the **b** axis, we can conclude that cooperative movements of complete columns of atoms are involved in the reaction.

The first step in the oxidation process of $Nb_{12}O_{29}$ seems to be the formation of lamellar defects, starting in the areas where the crystal has some stacking faults. The first movements of atoms giving rise to such defects is the creation of a (5×3) block, and the displacement of the block interface propagates in either direction, leading to ripples parallel to the **c** axis. To terminate the lamellar defect, (3×3) blocks were also formed.

A $Nb_{22}O_{54}$ structure was formed after further oxidation, showing black contrast between (3×3) and (4×3) blocks corresponding to Nb^{5+} occupying tetrahedral sites.

To proceed further in the oxidation process was quite difficult as specimen contamination did not allow us to distinguish clearly the subsequent changes in the structure. However, we have now carried out experiments following the oxidation process with a $Nb_{22}O_{54}$ sample as a starting material. The analysis of these results is in progress and will be presented in a future paper.

[2]Note that the **a** and **c** labeling of the published structures of $Nb_{12}O_{29}$ and $Nb_{22}O_{54}$ is interchanged; see diagrams in Figs. 1 and 8.

ACKNOWLEDGMENTS

We thank the EPSRC for financial support (ROPA Grant GR/K36492) and Professor B. Cantor for the provision of laboratory facilities.

REFERENCES

1. J. G. Allpress, J. V. Sanders, and A. D. Wadsley, *Phys. Status Solidi* **25,** 541 (1968).
2. J. M. Browne, J. L. Hutchison, and J. S. Anderson, *Proc. 7th Symp. React. Solids* **116** (1972).
3. J. S. Anderson, *Chem. Script.* **14,** 129 (1979).
4. R. C. Doole, G. M. Parkinson, J. L. Hutchison, M. J. Goringe, and P. J. F. Harris, *JEOL News* **30E,** 30 (1992); R. C. Doole, G. M. Parkinson, and J. M. Stead, Institute of Physics Conference Series, Vol. 118, 57, Institute of Physics, Bristol, 1991.
5. M. J. Sayagués and J. L. Hutchison, *J. Solid State Chem.* **124,** 116 (1996).
6. I. O. Bovin, D. X. Lee, L. Stemberg, and H. Annchcd, *Z. Kristallgr.* **168,** 98 (1984).
7. S. Horiuchi and S. Kimura, *Jpn. J. Appl. Phys.* **21,** L97 (1982).